Effects of nonlinearity on the optical diffraction of Bose-Einstein condensates: Direct integration of optically coupled multicomponent Gross-Pitaevskii equation

Taro Ando* and Yoshiyuki Ohtake
Hamamatsu Photonics K.K., Central Research Laboratory, Hirakuchi, Hamakita-ku, Hamamatsu 434-8601, Japan

Jun-ichi Kondo† and Katsuhiro Nakamura‡
Department of Applied Physics, Osaka City University, Sumiyoshi-ku, Osaka 558-8585, Japan
(Received 25 October 2010; published 28 February 2011)

We investigate in detail the effects of nonlinearity on optical diffraction of Bose-Einstein condensates (BECs). By directly integrating the optically coupled two-component Gross-Pitaevskii equation in real space-time, comprehensive analyses of BEC optical diffraction phenomena are done under various conditions of light-pulse irradiation, total number of BEC atoms, etc., without using the adiabatic elimination approximation for an atomic excited state. Calculation results for the optical diffraction of ^{87}Rb BECs revealed that (1) the effect of nonlinearity on the atomic states causes the "nonkinetic" nonlinear effect in the Raman-Nath regime of diffraction, while the dynamics of BEC atoms due to the nonlinearity-induced repulsive forces works dominantly to produce the "kinetic" nonlinear effect in the Bragg regime of diffraction; (2) nonlinearity reduces the amplitude and frequency of the two-photon Rabi oscillation between BEC stationary and moving states, suggesting limitations in implementing the BEC Mach-Zehnder interferometer; and (3) the observed nonlinear effects are free from kinetic effects of the atomic excited state and not responsible for the optical transition process.

DOI: 10.1103/PhysRevA.83.023619 PACS number(s): 03.75.−b, 42.50.Md, 37.10.Vz, 32.90.+a

I. INTRODUCTION

The interaction between light and matter is certainly an issue of fundamental interest in quantum physics. Above all, Bragg scattering of an atom from a standing light wave, which is realized by a two-photon Raman transition (TPRT) and is usually referred to as an optical Bragg diffraction (OBD), has been studied extensively over the past two decades in the context of atom optics [1–5]. More recently, Kozuma *et al.* [6] achieved a 50:50 beam splitter for Bose-Einstein condensates (BECs) using the OBD to advance the coherent matter-wave optics such as a Mach-Zehnder interferometer for BEC matter waves [7–9]. In practice, BEC experiments easily suffer from external disturbance, and thus theoretical predictions are helpful for evaluating the experimental results and extracting physically substantial information.

Theoretical descriptions of Raman coupling among BEC internal states have been studied extensively so far from the viewpoints of a BEC laser [10–13], output coupling for the BEC laser [14,15], relative phase measurement of two BEC species [16–21], electromagnetically induced transparency [22], and vortex coupler [23–32]. Optical diffraction of a BEC is the simplest example of BEC TPRT. Nevertheless, the effects of nonlinearity on the BEC's optical diffraction are far from obvious. While this subject was previously pursued in Ref. [33] in the context of an optically coupled, discrete three-level model consisting of initial, internal-excited, and final states of BEC, neither the spatiotemporal behaviors of a macroscopic wave function nor higher-order diffraction effects have been clarified.

In this paper, we investigate in detail the effects of nonlinearity on optical diffraction of ^{87}Rb BEC by directly solving optically coupled two-component (OCT) Gross-Pitaevskii equation (GPE) in real-space representation under realistic material parameters. Calculations of BEC optical diffraction under various conditions of nonlinearity and pulse duration revealed that the nonkinetic and kinetic nonlinear effects become dominant in the Raman-Nath and Bragg regimes of diffraction, respectively, and that nonlinearity reduces the amplitude and frequency of the two-photon Rabi oscillation between the BEC's stationary and moving states. Here, "nonkinetic" indicates the nonlinear effect brought by the changes in atomic states of BEC atoms, while "kinetic" means the one induced from the kinetic motions of BEC atoms due to interatomic repulsive forces. The observed phenomena are free from the kinetic effects of the atomic excited state and the effects of a nonlinear interaction term on the optical transition process, a fact which is deduced from the correspondence between the results via OCT-GPE and the adiabatic elimination approximation.

This paper is organized as follows. After establishing basic formulations in Sec. II, we describe in Sec. III the numerical procedure for solving an OCT-GPE and demonstrate examples involving the comparison between the results thus obtained and that available in the adiabatic elimination approximation [34,35]. In Sec. IV, calculation results for TPRT of ^{87}Rb BECs are presented for various conditions of nonlinearity and pulse-irradiation duration to discuss the effects of nonlinearity on the TPRT.

II. THEORETICAL MODEL FOR OPTICAL DIFFRACTION OF BEC

In this section, we describe a theoretical model of TPRT among the kinetic states of a BEC wave packet (WP). The

*taro@crl.hpk.co.jp
†Present address: Hamamatsu Photonics K.K., Electron Tube Division, 314-5 Shimokanzo, Iwata-City 438-0193, Japan.
‡Present address: Faculty of Physics, National University of Uzbekistan, Vuzgorodok, Tashkent 100174, Uzbekistan.

temporal evolution of the BEC WP under irradiation of light is formulated based on a macroscopic wave function of the BEC WP containing an internal degree of freedom, the formulation which is frequently seen in handling a multicomponent BEC system [23–27,29–32,34,35].

A. GPE with internal degree of freedom

We consider a BEC consisting of atoms, each of which contains two internal states. In the Schrödinger picture (indicated by the suffix "S"), the total wave function Φ_S is given as a function of spatial coordinates $\boldsymbol{r} = (x,y,z)$ and a temporal variable t in the $(3+1)$-dimensional space-time:

$$\Phi_S(\boldsymbol{r},t) = \phi_1(\boldsymbol{r},t) \otimes |1\rangle_S + \phi_2(\boldsymbol{r},t) \otimes |2\rangle_S \equiv \begin{pmatrix} \phi_1(\boldsymbol{r},t) \\ \phi_2(\boldsymbol{r},t) \end{pmatrix}, \tag{1}$$

where $|i\rangle_S$ is a ket vector expressing the internal states of BEC atoms with $i = 1$ for the ground state and $i = 2$ for the excited state. $\phi_i(\boldsymbol{r},t)$ corresponds to a macroscopic wave function of BEC in the ith internal state and represents the real-space dynamics of BEC WP. Here, Φ_S is normalized by the number of BEC atoms N_0, i.e.,

$$|\Phi_S|^2 = \int d^3\boldsymbol{r}[|\phi_1(\boldsymbol{r},t)|^2 + |\phi_2(\boldsymbol{r},t)|^2] = N_0.$$

The temporal development of Φ_S is described by the following two-component GPE:

$$i\hbar\frac{d}{dt}\Phi_S(\boldsymbol{r},t) = \hat{\mathcal{H}}_S\Phi_S(\boldsymbol{r},t), \tag{2}$$

where $\hbar$ is the Plank constant and the system's total Hamiltonian $\hat{\mathcal{H}}_S$ is expressed as an operator-component 2×2 matrix on the basis of the internal state:

$$\hat{\mathcal{H}}_S = \begin{pmatrix} \hat{H}_{11} & \hat{H}_{12} \\ \hat{H}_{21} & \hat{H}_{22} \end{pmatrix}. \tag{3}$$

The diagonal elements of $\hat{\mathcal{H}}_S$ are explicitly written as operators acting on the real-space coordinates:

$$\begin{aligned} \hat{H}_{11} &= -\frac{\hbar^2}{2m}\nabla^2 + u_{11}|\phi_1|^2 + u_{12}|\phi_2|^2, \\ \hat{H}_{22} &= -\frac{\hbar^2}{2m}\nabla^2 + \hbar\omega_{12} + u_{21}|\phi_1|^2 + u_{22}|\phi_2|^2, \end{aligned} \tag{4}$$

where m is atomic mass and $\hbar\omega_{12}$ (>0) is the energy difference between the internal ground and excited states. In Eq. (4), coefficients of the nonlinear interaction terms, u_{ij}, are defined as

$$u_{ij} = \frac{4\pi\hbar^2 a_{ij}}{m}, \tag{5}$$

with a_{ij} $(=a_{ji})$ as the s-wave scattering length between the atoms of the ith and jth states.

The off-diagonal part of the total Hamiltonian, $\hat{\mathcal{H}}_{\text{off-diag.}}$, describes the coupling between the internal ground and excited states, i.e., the light-BEC interaction term in the present study. $\hat{\mathcal{H}}_{\text{off-diag.}}$ is defined in the following section.

B. Two-component GPE with interaction terms due to standing light waves

Optical diffraction phenomena of BECs are caused by the interaction between BECs and a standing light wave [36]. The standing light wave is expressed as the sum of electric fields of two counter-propagating plane-wave lights, whose angular frequencies and wave numbers are ω_α and k_α $(\alpha = 1,\ 2)$, respectively. Here, we choose the propagation direction of lights as the x direction. Assuming that the electric-field amplitudes of the two lights are commonly E_0 and that both lights are linearly polarized in the z direction, the electric field of the standing light wave is written as

$$\begin{aligned} E(x,t) &= E_0\cos(k_1x - \omega_1t) + E_0\cos(-k_2x - \omega_2t) \\ &= 2E_0\cos\left(kx - \frac{\Delta\omega}{2}t\right)\cos\left(\omega t - \frac{\Delta k}{2}x\right), \end{aligned} \tag{6}$$

where we introduced $k = (k_1+k_2)/2$, $\Delta k = k_1 - k_2$, $\omega = (\omega_1+\omega_2)/2$, and $\Delta\omega = \omega_1 - \omega_2$ for notational simplicity.

The light-BEC interaction term is given as follows using a dipole moment operator $\hat{\mu}_z$:

$$\begin{aligned} &-\hat{\mu}_z E(x,t) \\ &= -2\mu_{12}\cos\left(kx - \frac{\Delta\omega}{2}t\right)\cos\left(\omega t - \frac{\Delta k}{2}x\right) \\ &\quad\times(|1\rangle\langle 2| + |2\rangle\langle 1|) \\ &= 2\hbar\Omega(x,t)\cos\left(\omega t - \frac{\Delta k}{2}x\right)\begin{pmatrix} 0 & 1 \\ 1 & 0 \end{pmatrix}, \end{aligned} \tag{7}$$

where

$$\begin{aligned} \mu_{12} &= \langle 1|\hat{\mu}_z|2\rangle = \langle 2|\hat{\mu}_z|1\rangle, \\ \Omega(x,t) &= -\frac{\mu_{12}E_0}{\hbar}\cos\left(kx - \frac{\Delta\omega}{2}t\right). \end{aligned} \tag{8}$$

Equation (7) indicates that the light-BEC interaction term corresponds to $\hat{\mathcal{H}}_{\text{off-diag.}}$.

Calculation of temporal evolution via Eq. (7) requires much computational cost because of the interaction term rapidly oscillating at the angular frequency of lights (ω). However, the rapid temporal dependence can be removed by introducing the Dirac-picture OCT-GPE with the choice of the noninteracting Hamiltonian $\hat{\mathcal{H}}_0$ as [37]

$$\hat{\mathcal{H}}_0 = \begin{pmatrix} 0 & 0 \\ 0 & \hbar\omega \end{pmatrix}.$$

The total Hamiltonian $\hat{\mathcal{H}}_D$ in the Dirac picture becomes

$$\hat{\mathcal{H}}_D = e^{i\hat{\mathcal{H}}_0t/\hbar}(\hat{\mathcal{H}} - \hat{\mathcal{H}}_0)e^{-i\hat{\mathcal{H}}_0t/\hbar} = \begin{pmatrix} \hat{H}'_{11} & \hat{H}'_{12} \\ \hat{H}'_{21} & \hat{H}'_{22} \end{pmatrix}, \tag{9}$$

with

$$\begin{aligned} \hat{H}'_{11} &= -\frac{\hbar^2}{2m}\nabla^2 + u_{11}|\phi_1|^2 + u_{12}|\phi_2|^2, \\ \hat{H}'_{22} &= -\frac{\hbar^2}{2m}\nabla^2 - \hbar\Delta_L + u_{21}|\phi_1|^2 + u_{22}|\phi_2|^2, \\ \hat{H}'_{12} &= \hat{H}'^{\dagger}_{21} = \hbar\Omega(x,t)\eta(x). \end{aligned} \tag{10}$$

In the above derivation, we neglected $e^{\pm i2\omega t}$ terms (rotating-wave approximation). In addition, a position-dependent

variable $\eta(x) = e^{-i\Delta kx/2}$ and an angular-frequency detuning $\Delta_L = \omega - \omega_{12}$ are introduced for notational simplicity. As a result, the Dirac-picture interaction term temporally oscillates at an angular frequency $\Delta\omega$, of which characteristic time scale is similar to that of the BEC motion in real space.

Along with the change of the Hamiltonian picture, the picture of internal wave functions also changes. This produces no superficial differences on the expressions regarding the space-time coordinates $(\boldsymbol{r},t)$, and thus OCT-GPE is reduced to the same form as Eq. (2) with only the subscript "S" changed to "D". In the following, we proceed with a discussion based on the Dirac-picture GPE and omit the subscript "D" and primes for simplicity.

Usually, OCT-GPE is reduced to the single-component GPE by adiabatically eliminating the excited state [34,35] under the assumption that $|\hbar\Delta_L|$ is large enough to be able to ignore the temporal change and kinetic energy of the excited state. For ^{87}Rb BEC, adiabatically eliminated single-component (AES) GPE is derived from Eq. (10) as follows:

$$i\hbar\frac{d}{dt}\phi_1(\boldsymbol{r},t) = -\frac{\hbar^2}{2m}\nabla^2\phi_1(\boldsymbol{r},t) + \left(u_{11}|\phi_1(\boldsymbol{r},t)|^2 + \frac{\hbar\Omega^2(x,t)\eta^2(x,t)}{\Delta_L}\right)\phi_1(\boldsymbol{r},t), \tag{11}$$

where we use the fact that the nonlinear interaction terms concerning the internal excited state vanish (see Sec. III B). AES-GPE enables simple treatment of BEC TPRT but fails when the excited-state contribution becomes significant, i.e., in the case of small $|\hbar\Delta_L|$, large nonlinearity, and intense light fields.

C. Optical diffraction of BEC via TPRT process

Figure 1 shows a schematic diagram of the BEC TPRT. All BEC atoms are assumed to be initially in the internal ground state with zero momentum [state (a)]. In Fig. 1, solid arrows and dashed arrows indicate absorption and induced emission of lights, respectively. The initial BEC WP undergoes the absorption and induced emission of two lights to transfer to a moving state [state (b)], which corresponds to the first-order diffraction state of BEC TPRT. Other diffraction states can also appear [e.g., a second-order diffraction state (c) and a -1st-order diffraction state (d)], but they are the minority under the Bragg diffraction condition, because ω_1 and ω_2 are adjusted so that the transition from (a) to (b) becomes a resonant TPRT. Here, a frequency detuning of the lights, $\Delta_L = \omega - \omega_{12}$ (<0), is chosen so that $|\Delta_L|$ is sufficiently large to suppress the single-photon transitions. However, a small portion of the BEC atoms can be observed in the internal excited states [(e), (f), and (g)], which will be discussed in Sec. III B.

Using the values in the interaction term [Eqs. (7) and (8)], "effective two-photon Rabi frequency" $\Omega_{\rm eff}$ is defined as the following [2]:

$$\Omega_{\rm eff} = -\frac{\Omega_0^2}{2\Delta_L} = -\frac{\mu_{12}^2E_0^2}{2\hbar^2\Delta_L}, \tag{12}$$

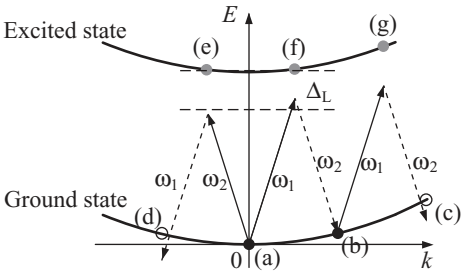

FIG. 1. Schematic diagram of BEC optical diffraction induced by two counterpropagating lights (angular frequencies are ω_1 and ω_2). The TPRT is detuned by angular frequencies of Δ_L from the resonant transition between the ground and excited states of BEC atoms. The TPRT attaches a momentum to a portion of the initially stationary BEC WP. (a) initial state, (b) first-order diffraction state, (c) second-order diffraction state, and (d) -1st-order diffraction state. (e), (f), (g): intermediate states in TPRT process.

where $\Omega_0 = -\mu_{12}E_0/\hbar$ is a Rabi (angular) frequency for the optical transition between the internal ground and excited states. When $\Omega_{\rm eff} \ll \hbar k^2/2m$ is satisfied, the TPRT causes the BEC optical diffraction phenomena in the Bragg regime. In this case, a 50:50 beam splitter for a BEC WP is achieved by irradiation of a $\pi/2$ pulse in the context of two-photon Rabi oscillation [8], where the duration τ of the $\pi/2$ pulse is defined as

$$\tau\Omega_{\rm eff} = \pi/2. \tag{13}$$

Equations (12) and (13) suggest that the $\pi/2$ pulses are realized for arbitrary pulse durations by choosing suitable light amplitudes E_0. In this study, the term "$\pi/2$-pulse duration" means the value of τ satisfying Eq. (13), and it is denoted as $\tau_{\pi/2}$. For a given $\tau_{\pi/2}$ value, irradiation of the $\pi/2$ pulse is numerically implemented by setting $E_0 = \hbar|\mu_{12}|\sqrt{(-\Delta_L)/(\pi\tau_{\pi/2})}$ during the time period from 0 to $\tau_{\pi/2}$ (otherwise, $E_0 = 0$).

III. NUMERICAL PROCEDURE

A. Time integration with exponential-operator expansion

To numerically integrate OCT-GPE, we apply an efficient, accurate, and stable time-integration method [38,39] based on the exponential-operator expansion (EPE) procedure [40,41] which leads to the split-step method. According to the EPE procedure, time evolution during a long time period $\tau = N\Delta t$ (N is a large integer number) can be achieved as a repeated application of N short-time evolutions. The short-time evolution of the wave function Φ is given as

$$\Phi(\boldsymbol{r},t+\Delta t) = \exp\left(-\frac{i}{\hbar}\frac{\Delta t}{2}\hat{K}\right)\exp\left(-\frac{i}{\hbar}\Delta t\hat{V}\left[\Phi';t+\frac{\Delta t}{2}\right]\right) \times \exp\left(-\frac{i}{\hbar}\frac{\Delta t}{2}\hat{K}\right)\Phi(\boldsymbol{r},t), \tag{14}$$

with

$$\Phi' = \exp\left(-\frac{i}{\hbar}\frac{\Delta t}{2}\hat{K}\right)\Phi(\boldsymbol{r},t), \tag{15}$$

where $\hat{K}$ and $\hat{V}$ are the kinetic and interaction parts of the total Hamiltonian $\hat{\mathcal{H}}$, respectively. We note that the above formula is derived from the second-order symmetric decomposition formula [41], and that Eq. (14) is valid even when $\hat{V}$ depends on Φ [38].

In practical calculations, the exponential of $\hat{K}$ is further decomposed by applying the space-splitting procedure [39,42,43]. On the other hand, the exponential of $\hat{V}$ can be expressed analytically without further decompositions. To show this, it is convenient to express the action of $\hat{V}$ as a 2×2 matrix acting locally on a pair of internal wave functions because $\hat{V}$ is a diagonal operator in the coordinate representation and operates independently at each point. A matrix expression of the interaction part $\hat{V}$ is written at each position as

$$\hat{V}[\Phi;t] = \begin{pmatrix} V_{11}[\Phi] & V_{12}(t) \\ V_{21}(t) & V_{22}[\Phi] \end{pmatrix}, \tag{16}$$

with

$$\begin{aligned} V_{11}[\Phi] &= u_{11}|\phi_1|^2 + u_{12}|\phi_2|^2, \\ V_{22}[\Phi] &= -\hbar\Delta_{\mathrm{L}} + u_{21}|\phi_1|^2 + u_{22}|\phi_2|^2, \\ V_{12}(t) &= V_{21}^*(t) = \hbar\Omega(x,t)\eta(x). \end{aligned} \tag{17}$$

In Eqs. (16) and (17), the functional dependence of V_{ij} is explicitly written to easily grasp the effect of each component while omitting the dependence of ϕ_i, Ω, and η on the space-time coordinates for notational simplicity.

Equation (17) indicates that $\hat{V}$ is a Hermitian matrix, hence $\hat{V}$ is diagonalized with the help of a unitary matrix U to give a diagonal matrix of which elements are expressed as

$$E_i = \frac{(V_{11}+V_{22}) \pm \sqrt{(V_{11}-V_{22})^2 + 4\hbar^2\Omega^2}}{2} \quad (i = 1, 2). \tag{18}$$

E_1 and E_2 correspond to "+" and "−" in the $\pm$ symbol, respectively. The final expression for the exponential of $\hat{V}$ becomes

$$\begin{aligned} \exp\left(-\frac{i\Delta t}{\hbar}\hat{V}\right) &= U^\dagger \begin{pmatrix} \exp(-iE_1\Delta t/\hbar) & 0 \\ 0 & \exp(-iE_2\Delta t/\hbar) \end{pmatrix} U \\ &= \begin{pmatrix} \hbar^2\Omega^2(\gamma_1+\gamma_2) & -\hbar\Omega\eta[(V_{11}-E_1)\gamma_1 + (V_{11}-E_2)\gamma_2] \\ -\hbar\Omega\eta^*[(V_{11}-E_1)\gamma_1 + (V_{11}-E_2)\gamma_2] & (V_{11}-E_1)^2\gamma_1 + (V_{11}-E_2)^2\gamma_2 \end{pmatrix}, \end{aligned} \tag{19}$$

where

$$\begin{aligned} \gamma_i &= e^{-i\Delta t E_i/\hbar}/|\mathcal{N}_i|^2\mathcal{N}_i \\ &= \sqrt{(V_{11}-E_i)^2 + \hbar^2\Omega^2} \quad (i = 1, 2). \end{aligned} \tag{20}$$

Equation (19) fails in the absence of external lights because either $\mathcal{N}_1$ or $\mathcal{N}_2$ becomes zero. However, in this case, $V_{12}(t)$ in Eq. (16) vanishes and the exponential of $\hat{V}$ is given as the first line of Eq. (19) with U as a unit matrix.

B. Numerical conditions and examples

We apply the developed method to the TPRT of a BEC WP. For direct comparison with experimental results [7–9], all results in the present study were obtained by applying the realistic material parameters of ^{87}Rb shown in Table I [44,45].

TABLE I. Parameters of ^{87}Rb in the present study. All values except for s-wave scattering length (a_{11}) are listed in Ref. [44].

Parameters	Values
m	$1.443\,160\,60(11)\times 10^{-25}$ kg
ω_{12}	$2\pi\,384.230\,484\,468\,5(62)$ THz
μ_{12}	$-3.584(4)\times 10^{-29}$ Cm
a_{11}	5.5 nm[a]

[a]Ref. [45].

The ground and lowest excited states of ^{87}Rb are $5^2S_{1/2}$ and $5^2P_{3/2}$ states, respectively, and the resonant transition between them is referred to as the D_2 transition.

Regarding the nonlinear-interaction coefficients, we employ an approximation in Ref. [33] that the nonlinear interactions involving the lowest excited state are negligible. Hence, u_{11} is determined from a_{11} (Table I) through Eq. (5), while others are determined as $u_{22} = u_{12} = u_{21} = 0$. This means that the nonlinear interaction term in GPE [Eq. (4)] induces repulsive forces only among ground-state ^{87}Rb atoms.

Discretization of space-time is also significant in numerical calculations. Since the light-BEC interaction term spatially varies with the pitch of the light's wavelength, space division must be sufficiently fine so that the spatial variation of the interaction term is correctly reproduced. Since the light's wavelength is approximately 780 nm for ^{87}Rb BECs, the spatial mesh size was chosen as $\Delta x = 25$ nm in the propagation direction but $\Delta y = \Delta z = 1\ \mu$m in the other directions [46]. The short-time evolution interval Δt is also determined once the spatial mesh size is given: We chose $\Delta t = 0.2\ \ \mu$s to satisfy the criterion $\hbar\Delta t/(m\Delta x^2) < 0.5$, which ensures the validity of the space-splitting procedure for the kinetic-energy term in the Hamiltonian [47]. The total number of points is chosen differently according to the purpose; e.g., $16\,000\times 200\times 200$ points (corresponding to a spatial regime of $400\times 200\times 200\ \mu$m^3) for demonstrating

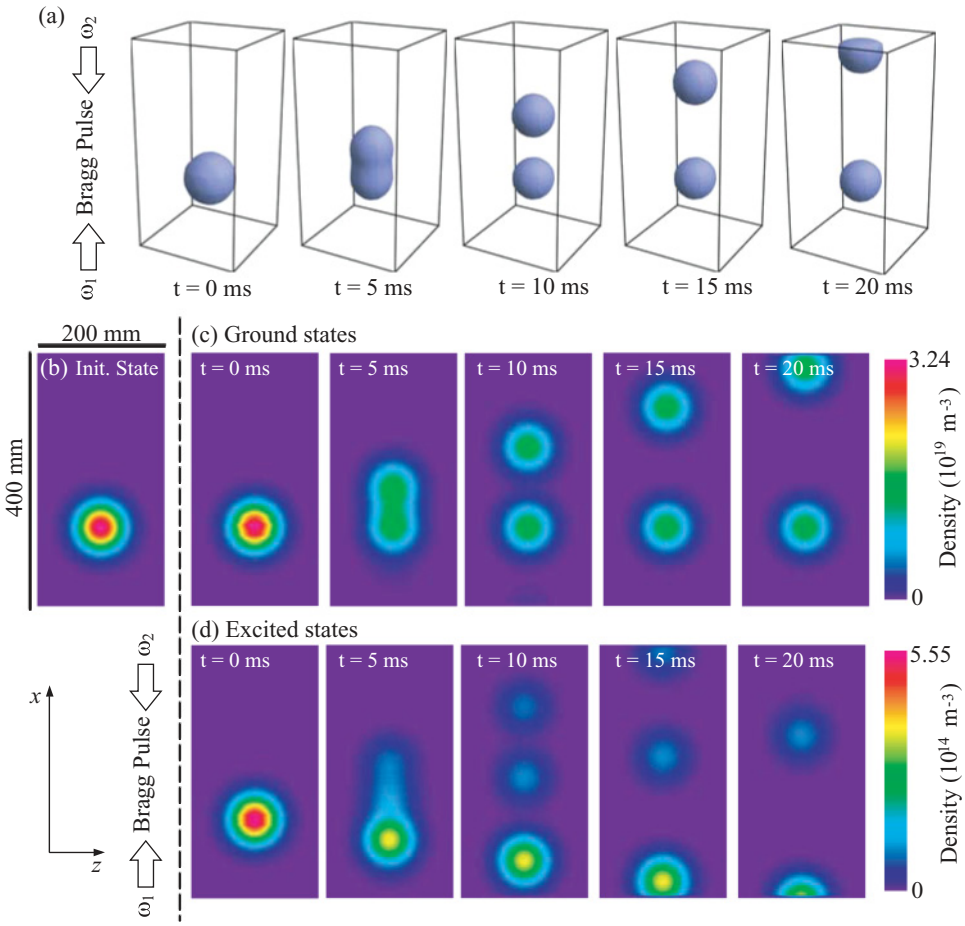

FIG. 2. (Color online) Temporal developments of an initially spherical Gaussian WP of ^{87}Rb BEC after irradiation of a $\pi/2$ Bragg pulse. The $\pi/2$ Bragg pulse is detuned from the D_2 transition by $\Delta_L/2\pi = -2$ GHz, and its duration is $\tau_{\pi/2} = 50$ μs. The initial BEC WP contains $N_0 = 10^5$ ^{87}Rb atoms. (a) Isosurface plots for density distributions of BEC WP. The isosurfaces represent $1/e^2$-density surfaces with respect to the maximum density of the initial WP. (b) Initial state. (c) Temporal snapshots of cross-sectional density distributions (on $y = 0$ plane) of the ground-state atoms after radiation of the $\pi/2$ Bragg pulse. (d) Same as (c), but for the excited-state atoms. Color bars at the right sides of (c) and (d) indicate the atom densities of the ground and excited states, respectively. In (c) and (d), $t = 0$ indicates the moment when the Bragg pulse irradiation has finished.

real-space dynamics of BEC WPs, or $32\,000 \times 200 \times 200$ points ($800 \times 200 \times 200$ μm^3) for quantitative analyses of the BEC momentum distribution.

We demonstrate an example for the dynamics of a BEC WP under a $\pi/2$ Bragg pulse. The angular frequencies of light for producing the Bragg pulse are determined as follows for a given frequency detuning Δ_L:

$$\omega_1 = (\omega_{12} + \Delta_L)\left[1 + \frac{\hbar(\omega_{12} + \Delta_L)}{mc^2}\right],$$
$$\omega_2 = (\omega_{12} + \Delta_L)\left[1 - \frac{\hbar(\omega_{12} + \Delta_L)}{mc^2}\right], \quad (21)$$

where c is the speed of light in a vacuum. Calculation conditions are chosen to reproduce practical experiments [7–9]. The BEC WP is assumed to be initially in a spherically symmetric Gaussian shape, whose radius is 50 μm (the radius is defined as the distance from the center to the sphere on which the density of the BEC atom becomes $1/e^2$ relative to that at the center). We also assume that the BEC WP contains $N_0 = 10^5$ ^{87}Rb atoms. The Bragg pulse is detuned from the D_2 transition by $\Delta_L/2\pi = -2$ GHz, and its duration is chosen as $\tau_{\pi/2} = 50$ μs. Figure 2(a) shows snapshots of the isosurface that illustrate the temporal development of the ground-state BEC WP after irradiation of the $\pi/2$ Bragg pulse. The time interval between adjacent snapshots is equally 5 ms, and the isosurfaces represent points where the density of the BEC atom becomes $1/e^2$ relative to the maximum density value in the initial Gaussian BEC WP [Fig. 2(b)]. Figure 2(c) shows snapshots of a cross-sectional density profile corresponding to Fig. 2(a), while Fig. 2(d) shows those of the excited-state component.

The present calculation method can predict the behavior of excited-state BEC WPs, which has been ignored in AES-GPE [34,35]. In the $t = 0$ snapshot of Fig. 2(d), approximately 0.01% of the total BEC atoms remain in the excited state. We observe in Fig. 2(d) three diffraction components in the excited state. Among them, the diffraction component corresponding to state (e) in Fig. 1 is dominantly observed, which is explained as follows. In Fig. 1(a),→(f)→(b) is a resonant transition and the occupation at (f) is efficiently transferred to (b), while the transition (a)→(e)→(d) is detuned, and the population of the final state (d) should become smaller than that of (b). As a result, a larger number of atoms should remain in the internal excited state (e) than in state (f).

C. Comparison of OCT-GPE with AES-GPE

Before proceeding to the study on the effects of nonlinearity, we describe the comparison between OCT-GPE and AES-GPE, which will help clarify the origin of the nonlinear effects. Strictly speaking, the nonlinear interaction is expressed in terms of the local density of the BEC atom. However, for simplicity, we use the total number of ^{87}Rb atoms (N_0) as a measure of the strength of nonlinearity while fixing the initial shape of BEC WP. Calculation conditions are chosen similarly as in Sec. III B unless otherwise stated.

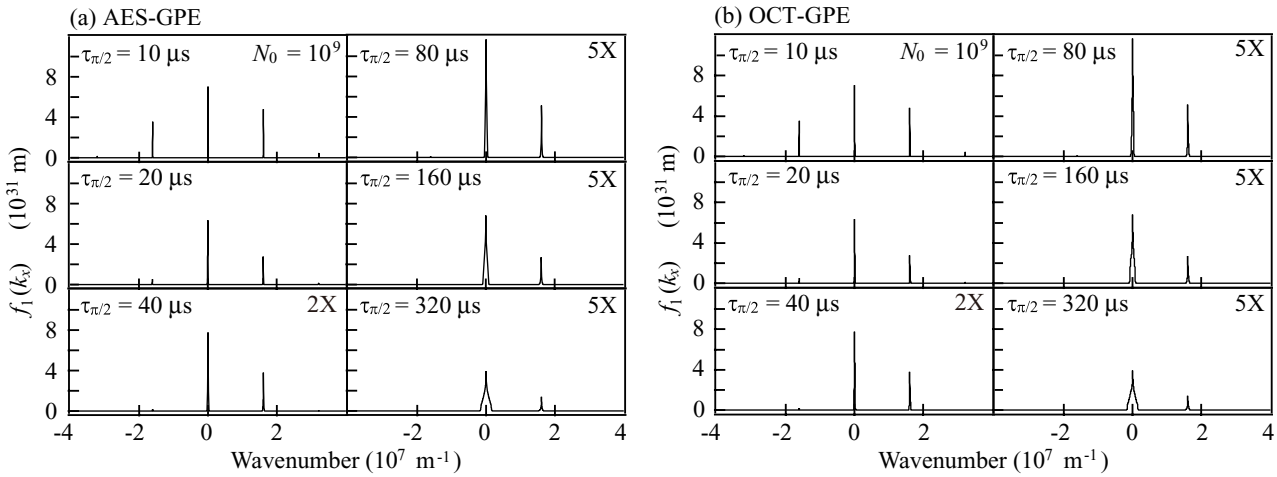

FIG. 3. k_x spectra of the ground-state BEC WP after TPRT calculated via (a) AES-GPE and (b) OCT-GPE: light-irradiation duration is $\tau_{\pi/2} = 10$, 20, 40, 80, 160, and 320 μs. The number of ^{87}Rb atoms in a BEC WP is $N_0 = 10^9$, and the frequency detuning of light pulses is $\Delta_L/2\pi = -2$ GHz.

To analyze the diffraction phenomena of the BEC WP in a quantitative manner, we define the x-directional wave-number distribution of the BEC WP as

$$f_i(k_x) = \iint_{-\infty}^{\infty} dydz|\tilde{\phi}_i(k_x; y,z)|^2, \tag{22}$$

where

$$\tilde{\phi}_i(k_x; y,z) = \frac{1}{\sqrt{2\pi}} \int_{-\infty}^{\infty} dx e^{-ik_x x} \phi_i(x,y,z) \tag{23}$$

is an x-directional Fourier spectrum of the BEC WP's wave function. In Eq. (23), the suffix i labels the internal state of ^{87}Rb atom as $i = 1$ for $5^2S_{1/2}$ state and $i = 2$ for $5^2P_{3/2}$ state. Equation (22) has the meaning of a momentum distribution of a BEC WP, hence it is referred to as a k_x spectrum in the following.

Figure 3 shows the k_x spectra just after TPRT calculated via AES-GPE and OCT-GPE for $N_0 = 10^9$. The k_x spectra are obtained for over $-1.26 \times 10^8 \leqslant k_x \leqslant 1.26 \times 10^8$ (m^{-1}) under the present space-division condition, but the displayed k_x ranges were restricted to observe in detail the lower-order diffraction components of BEC OBD. We note that no visual higher-order peaks are available in the omitted k_x regimes. Although Fig. 3 is obtained under the largest nonlinearity condition where the maximal difference between OCT-GPE and AES-GPE is expected, we find only minor differences in numeric with no observable differences between the two k_x spectra. In fact, the correspondence is also confirmed for $N_0 \leqslant 5 \times 10^8$, meaning that OCT-GPE and AES-GPE produce nearly identical k_x spectra under the present calculation conditions. This also agrees with the fact that the population of the excited state ^{87}Rb is at most 0.01% in number for all calculations.

It is noted that AES-GPE was derived by omitting the excited-state contribution in OCT-GPE, and that the nonlinear interaction and light-BEC coupling was reduced to an effective potential acting only on a wave function of the ground-state BEC WP [Eq. (11)]. The correspondence between the k_x spectra via OCT-GPE and AES-GPE indicates that the nonlinear effects in the k_x spectra are free from the effects dropped in AES-GPE; i.e., the kinetic effect of the excited-state BECs and the nonlinear effect on the optical transition process between the atomic states of BECs.

It is meaningful to examine the criterion for failure of AES-GPE. As mentioned in the end of Sec. II B, AES-GPE can fail in the case of small Δ_L. Figures 4(a) and 4(b), respectively, show k_x spectra for the ground-state BEC WP calculated via AES-GPE and OCT-GPE with varying Δ_L while fixing $N_0 = 10^8$ and $\tau_{\pi/2} = 40$ μs. AES-GPE hardly produces visual change in the k_x spectra with varying Δ_L (in fact, k_x spectrum via AES-GPE is nearly identical for $\Delta_L = -2 \times 10^4 \sim -2 \times 10^9$ Hz), while OCT-GPE gives different k_x spectra in the small Δ_L regime: The slight increase of zeroth-order diffraction peak and decrease of the first-order diffraction peak appear when Δ_L is reduced from -800 to -200 kHz. In terms of the population of the internal excited state, the spectral change is observed for $N_{ex} \geqslant 2.1\%$ but not for $N_{ex} \leqslant 0.47\%$, suggesting that AES-GPE starts to fail around $N_{ex} \approx 1\%$. Moreover, the decrease of both zeroth- and first-order diffraction peaks appears for $N_{ex} \geqslant 10\%$, and AES-GPE completely deviates from OCT-GPE in this regime.

Effects of nonlinearity and light-pulse amplitude on the failure of AES-GPE are also interesting but too complicated to be clarified in the present study, hence we only introduce two examples suggesting the effects. Figures 4(c) and 4(d) demonstrate the deviation of AES-GPE from OCT-GPE due to large nonlinearity and light-pulse amplitude, respectively. We note that the light-pulse amplitude relates to the light-pulse duration via Eqs. (12) and (13), meaning that a small $\tau_{\pi/2}$ corresponds to a large light-pulse amplitude. Anyway, both nonlinearity and light-pulse amplitude can enhance the excited-state population to cause the deviation of AES-GPE from OCT-GPE.

IV. RESULTS AND EFFECTS OF NONLINEARITY

A. Momentum spectra of macroscopic wave functions after light irradiation

Effects of nonlinearity are clarified from the behavior of the k_x spectra under various conditions of nonlinearity and

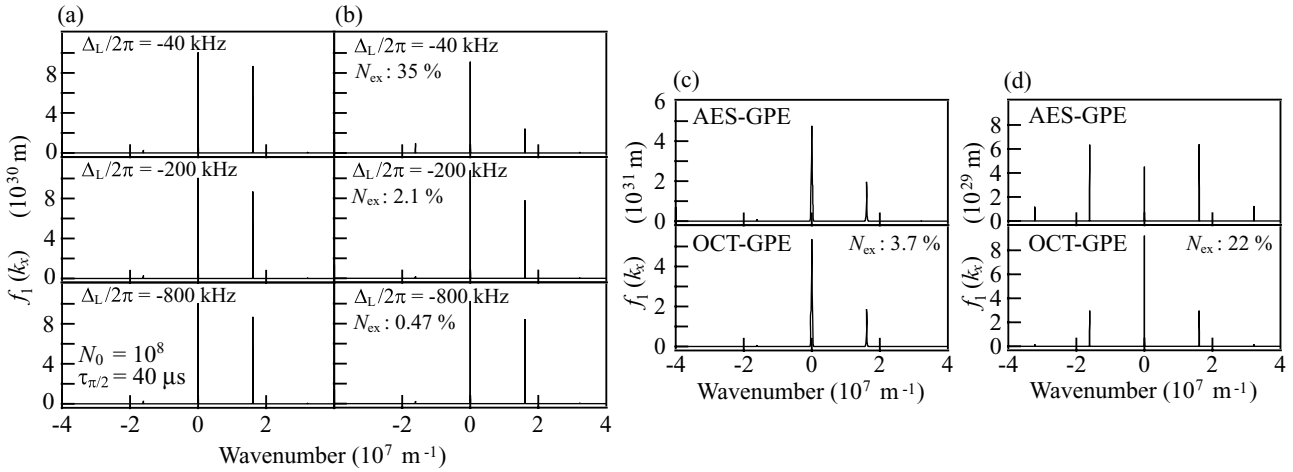

FIG. 4. Comparison between k_x spectra of the ground-state BEC WP calculated via (a) AES-GPE and (b) OCT-GPE under various frequency detunings ($\Delta_L = -40$, -200, and -800 kHz) while fixing other conditions as $N_0 = 10^8$ and $\tau_{\pi/2} = 40$ μs. And comparison between the k_x spectra via AES- and OCT-GPE under the conditions of (c) $\Delta_L = -200$ kHz, $N_0 = 2 \times 10^9$, and $\tau_{\pi/2} = 40$ μs, and (d) $\Delta_L = -200$ kHz, $N_0 = 10^7$, and $\tau_{\pi/2} = 2$ μs. N_{ex} indicates the ratio of atoms in the internal excited state.

light-pulse duration. Figures 5 and 6 exhibit k_x spectra of the ground-state BEC WP for $N_0 = 10^7$ and 10^8, respectively. In Figs. 3, 5, and 6, the k_x spectra exhibit the properties of two types of diffraction phenomena according to whether the $\pi/2$-pulse duration $\tau_{\pi/2}$ exceeds 20 μs. The k_x spectra for $\tau_{\pi/2} = 10$ μs are assigned to the Raman-Nath regime of diffraction due to the appearance of the comparative zeroth- and $\pm$1st-order diffraction peaks. On the other hand, k_x spectra for $\tau_{\pi/2} \geqslant 40$ μs exhibit the properties of the Bragg regime of diffraction, where light pulses provide the function of a 50:50 beam splitter for a BEC WP.

Here, we note that the k_x spectra present no visual difference for $\tau_{\pi/2} \geqslant 40$ μs in Fig. 5. On the other hand, decreases in spectral peaks for $\tau_{\pi/2} \geqslant 80$ μs are commonly observed in Figs. 3 and 6, both of which are obtained under large nonlinearity conditions. Finally, the nonlinearity-induced decrease of the first-order diffraction peak becomes prominent for $N_0 \geqslant 10^8$ under the present calculation condition. Moreover, Fig. 3 shows a growing change in spectral shape with the increase of $\tau_{\pi/2}$. To study in detail this property specific to the large nonlinearity condition, we plot the spectral widths of zeroth and first-order diffraction peaks as functions of $\tau_{\pi/2}$ in Fig. 7(a). The spectral peak corresponding to the stationary state exhibits prominent broadening as the nonlinearity increases, while the moving state shows only minor broadening. This fact is consistent with the property of the nonlinear interaction in ^{87}Rb BEC; i.e., repulsive forces work only among ground-state ^{87}Rb atoms.

Figures 7(b) and 7(c) exhibit magnified k_x spectra around $k_x \approx 0$ for $\tau_{\pi/2} = 10$ and 320 μs, respectively, in the case of $N_0 = 10^9$. The k_x spectrum appears to keep the initial Gaussian shape for $\tau_{\pi/2} = 10$ μs, while it presents spectral broadening associated with an apparent shape change for $\tau_{\pi/2} = 320$ μs. Since the spectral broadening is hardly observed under small nonlinearity (Figs. 5 and 6), the broadening is attributed to an effect of nonlinearity. From another point of view, the spectral broadening can be explained by the kinetic motion of the ground-state BEC due to repulsive forces among ^{87}Rb atoms. In fact, the spectral broadening is hardly seen for $\tau_{\pi/2} < 40$ μs,

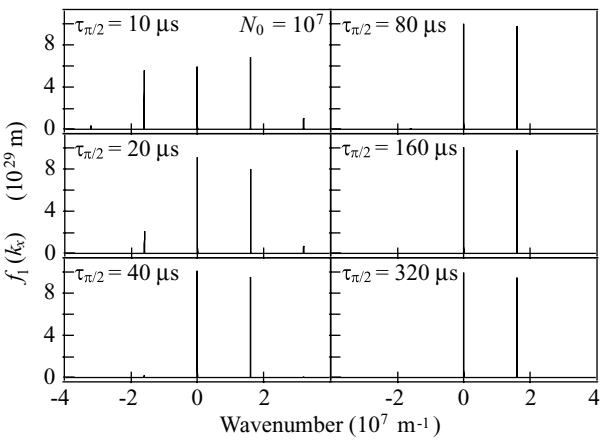

FIG. 5. k_x spectra of the ground-state BEC WP after TPRT: light-irradiation duration is $\tau_{\pi/2} = 10$, 20, 40, 80, 160, and 320 μs. The number of ^{87}Rb atoms in a BEC WP is $N_0 = 10^7$, and TPRT is detuned by $\Delta_L/2\pi = -2$ GHz from the D_2 transition of ^{87}Rb.

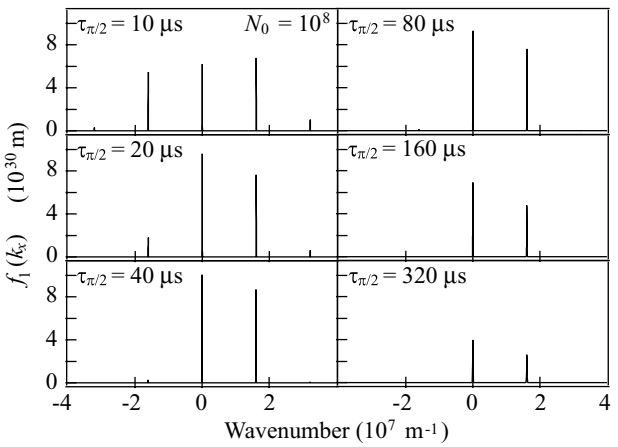

FIG. 6. Same as Fig. 5, but for $N_0 = 10^8$.

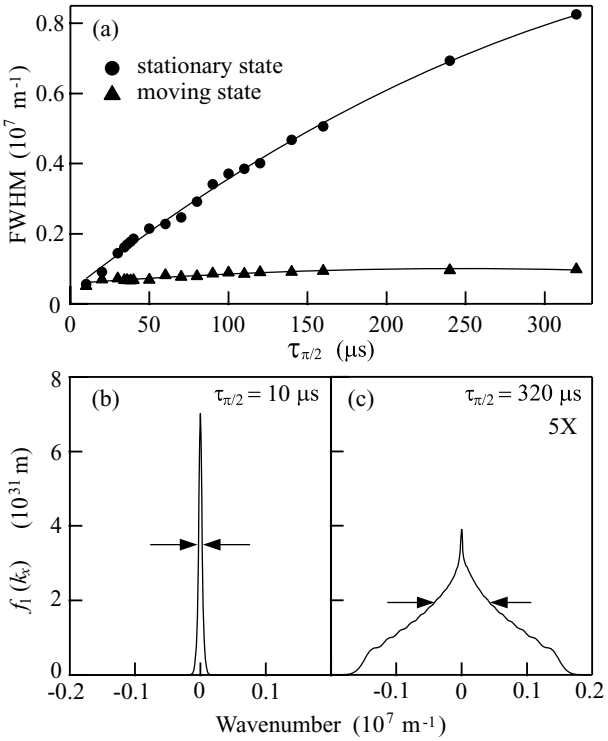

FIG. 7. (a) Change in full-width at half-maximum of the k_x-spectrum peaks corresponding to the stationary (circle) and moving (triangle) states against $\tau_{\pi/2}$. Solid curves are eye guides. (b), (c): k_x spectra magnified around $k_x \approx 0$ for (b) $\tau_{\pi/2} = 10$ μs and (c) $\tau_{\pi/2} = 320$ μs. All results are calculated under $N_0 = 10^9$.

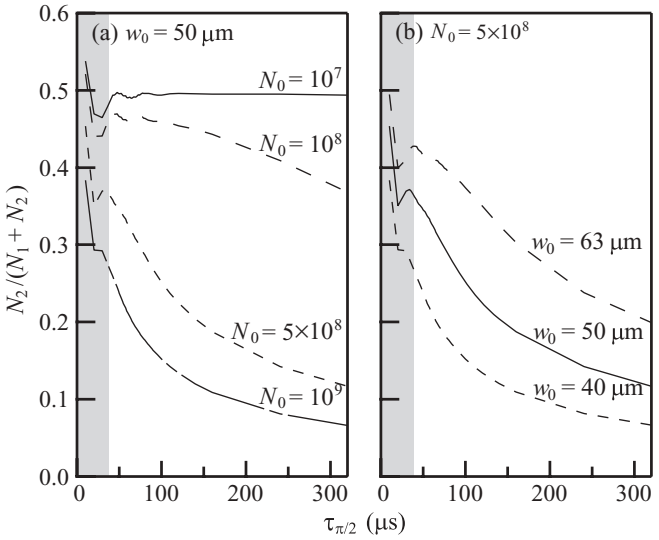

FIG. 8. Changes in reflectivity R [$=N_2/(N_1+N_2)$] against $\tau_{\pi/2}$ in BEC TPRT for (a) total atom number of $N_0 = 10^7$, 10^8, 5×10^8, and 10^9 while fixing the size of BEC WP as $w_0 = 50$ μm, and for (b) BEC WP sizes of $w_0 = 40$, 50, and 63 μm while fixing the total atom number as $N_0 = 5 \times 10^8$. The shaded areas indicate the Raman-Nath regime of diffraction.

suggesting that at least more than 40 μs of light irradiation is required for each BEC atom to acquire momentum from the interatomic repulsive forces. Finally, the spectral broadening in Fig. 7(c) is mainly caused by a "kinetic nonlinear effect," which can be observed in the Bragg diffraction regime.

On the other hand, nonlinearity also induces a nonkinetic effect due to a position-dependent energy shift of the internal ground state [Eq. (4)]. However, it is difficult to separate the nonkinetic effect from the kinetic one in the k_x spectra for larger $\tau_{\pi/2}$ regimes. Recalling that the initial Gaussian spectral shape was almost kept in Fig. 6(b), the k_x spectrum suffers from little kinetic nonlinear effect under the condition of $\tau_{\pi/2} = 10$ μs even when $N_0 = 10^9$. Hence, the reduction of the $\pm$1st-order diffraction peaks in the $\tau_{\pi/2} = 10$ μs spectrum in Fig. 3(b) should be specified as a nonkinetic nonlinear effect. Roughly speaking, the nonkinetic nonlinear effect appears in the Raman-Nath regime of diffraction, while the kinetic nonlinear effect becomes dominant in the Bragg regime of diffraction.

B. Beam-splitting characteristics of $\pi/2$ Bragg pulse

In Figs. 3, 5, and 6, we observe a monotonous decrease in the first-order diffraction peaks with the increase of $\tau_{\pi/2}$ ($\geqslant$80 μs). The decrease in the spectral peak is associated with spectral broadening, and thus the number of BEC atoms in the stationary and moving states must be evaluated to quantitatively investigate the beam-splitting property of the $\tau_{\pi/2}$ Bragg pulse. The atom number in a particular kinetic state is available by integrating the k_x spectrum with respect to k_x over a suitable integral domain around the corresponding spectral peak. Using the k_x spectrum for the internal ground state [given in Eq. (22) while setting $i = 1$], we define the number of ground-state atoms in the stationary ($j = 1$) and moving ($j = 2$) states as

$$N_j = \int_{k_j^{\rm peak}-\Delta\kappa}^{k_j^{\rm peak}+\Delta\kappa} dk_x\, f_1(k_x) \quad (j = 1,2), \tag{24}$$

where the center of the integral domain is chosen as the corresponding spectral-peak position ($k_1^{\rm peak} = 0.0$ and $k_2^{\rm peak} = 1.7 \times 10^7$) with the half-width of the integral domain as $\Delta\kappa = 8.0 \times 10^6$.

The transfer ratio from the stationary to moving state, i.e., the "reflectivity" of a BEC-OBD beam splitter, is determined as $R = N_2/(N_1 + N_2)$ using Eq. (24). Figure 8(a) exhibits the changes of R against $\pi/2$-pulse duration for $N_0 = 10^7$, 10^8, 5×10^8, and 10^9, while fixing the size of BEC WP as $w_0 = 50$ μm. The behavior of R against $\tau_{\pi/2}$ becomes similar for $N_0 \leqslant 10^7$, which suggests a criterion for linear regimes. In fact, the behavior of R for $N_0 = 10^7$ in Fig. 8(a) indicates that a 50:50 beam splitter is achieved for over $\tau_{\pi/2} \geqslant 40$ μs. On the other hand, we observe growing decreases in R with increasing $\tau_{\pi/2}$ for $N_0 \geqslant 10^8$. The decreases in R are enhanced by the increase of N_0, indicating the failure of a $\pi/2$ Bragg pulse as a 50:50 beam splitter under large nonlinearity conditions.

On the other hand, Fig. 8(b) exhibits the changes of R against $\pi/2$-pulse duration for BEC WP sizes of $w_0 = 40$, 50, and 63 μm while fixing the total atom number as $N_0 = 5 \times 10^8$. It is noted that $w_0 = 40$ and 63 μm are $1/\sqrt[3]{2}$ and $\sqrt[3]{2}$ times as large as $w_0 = 50$ μm, respectively, meaning that the maximum atom density in BEC WP is varied by a factor of 2 without the change of N_0. In Fig. 8(b), the decrease of w_0 with a fixed N_0 presents a similar effect to that induced by the increase

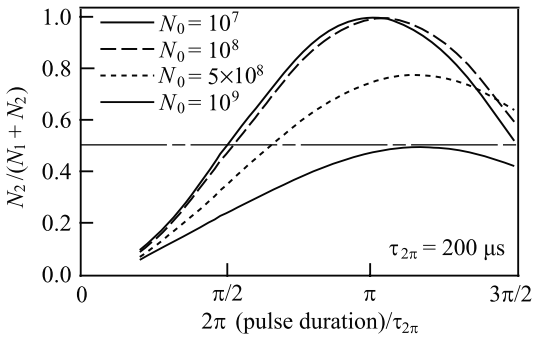

FIG. 9. Changes in two-photon Rabi oscillation between stationary and moving states of a ground-state BEC WP according to the strength of nonlinearity.

of N_0 with fixed w_0 in Fig. 8(a). This observation indicates that the effects of nonlinearity are determined predominantly by the maximum atom density in BEC WP rather than by the total atom number under the present conditions.

C. Effects of nonlinearity on two-photon Rabi oscillation

Regarding optical transition in a semiconductor material, a Rabi frequency is known to change due to nonlinearity (the shifted Rabi frequency is sometimes referred to as a renormalized Rabi frequency, e.g., Ref. [48]). A similar effect is expected in BEC OBD to produce the superficial decreases in R at $\pi/2$-pulse conditions as in Fig. 8. Therefore, it is necessary to study two-photon Rabi oscillations of BECs under large nonlinearity for determining the proper pulse-irradiation conditions of a 50:50 BEC beam splitter.

To study the nonlinearity-induced frequency shift of the two-photon Rabi oscillation, we calculate the reflectivity R in the BEC OBD phenomenon for various pulse-irradiation durations. Previously, light pulses were applied while maintaining the $\pi/2$-pulse irradiation condition, i.e., by adjusting the amplitudes of light pulses for the desired $\pi/2$-pulse duration. Here, light pulses are applied while varying the pulse irradiation time, which does not always satisfy the $\pi/2$-pulse irradiation condition, by fixing the light amplitudes so that the 2π-pulse duration is 200 μs. Figure 9 shows the two-photon Rabi oscillation between stationary and moving states of a ground-state BEC WP for various strengths of nonlinearity.

We observe in Fig. 9 two types of nonlinear effects on the two-photon Rabi oscillation between the BEC kinetic states: one is the shift of the Rabi frequency similar to the renormalized Rabi frequency in a semiconductor material, and the other is the decreased amplitude of the two-photon Rabi oscillation. Due to these nonlinear effects, irradiation of $\sim 1.2\pi$ pulse is required to achieve a 50:50 beam splitter for the BEC WP in the case of $N_0 = 10^9$. Moreover, Fig. 9 shows that a π Bragg pulse becomes practically unavailable for $N_0 \geqslant 5 \times 10^8$. These results suggest a limitation in constructing a Mach-Zehnder interferometer for BEC-matter waves with the help of BEC OBD under large nonlinearity conditions. The failure of the BEC Mach-Zehnder interferometer occurs for large nonlinearity exceeding a thousand times its value in typical experiments (for ^{87}Rb BEC, $N_0 \sim 10^5$), and this condition can be achieved by increasing N_0, reducing the size of the initial BEC WP, and enhancing the s-wave scattering length a_{11} via the Feshbach resonance.

V. SUMMARY AND CONCLUSION

In this paper, we investigated in detail the effects of nonlinearity on the optical diffraction phenomena of a BEC WP. To enable comprehensive analyses of BEC optical diffraction phenomena under a variety of conditions, we developed a numerical method based on the direct integration of OCT-GPE in real space-time. The calculation results for optical diffraction of ^{87}Rb BEC WPs revealed that the nonkinetic nonlinear effect appears in the Raman-Nath regime of diffraction, while the kinetic nonlinear effect becomes dominant in the Bragg regime of diffraction. Regarding the Bragg diffraction regime, it was shown that (1) while the reflectivity of BEC-OBD beam splitter guarantees 50:50 population suited to an ideal $\pi/2$ Bragg pulse in a wide range of $\tau_{\pi/2} \geqslant 40$ μs under the small nonlinearity condition ($N_0 \leqslant 10^7$), it decreases with increasing $\tau_{\pi/2}$ under the large nonlinearity condition ($N_0 \geqslant 10^8$) and this tendency is enhanced by the increase of N_0; (2) the nonlinearity reduces amplitude and frequency of the two-photon Rabi oscillation between the BEC kinetic states, suggesting limitations for constructing a BEC Mach-Zehnder interferometer under large nonlinearity exceeding a thousand times its value in typical experiments for ^{87}Rb BECs. The effects of nonlinearity reported in the present study were also reproduced via an effective single-component GPE that was derived from OCT-GPE based on the adiabatic elimination approximation, indicating that the effects are free from kinetic effects of the atomic excited state and not responsible for the optical transition process. The present numerical method is effective for the analysis of BEC TPRT even when the population of the internal excited state exceeds 1%, where AES-GPE fails to give quantitative results.

ACKNOWLEDGMENTS

The authors thank T. Hiruma, A. Hiruma, Y. Suzuki, T. Hara, and S. Ohsuka of Hamamatsu Photonics K.K. for their encouragement throughout this work, as well as the anonymous reviewer for important comments on the role of the comparison between OCT- and AES-GPE.

[1] P. J. Martin, B. G. Oldaker, A. H. Miklich, and D. E. Pritchard, Phys. Rev. Lett. **60**, 515 (1988).
[2] D. M. Giltner, R. W. McGowan, and S. A. Lee, Phys. Rev. A **52**, 3966 (1995).
[3] M. K. Oberthaler, R. Abfalterer, S. Bernet, J. Schmiedmayer, and A. Zeilinger, Phys. Rev. Lett. **77**, 4980 (1996).
[4] S. Kunze, S. Dürr, and G. Rempe, Europhys. Lett. **34**, 343 (1996).

[5] S. Dürr and G. Rempe, Phys. Rev. A **59**, 1495 (1999).
[6] M. Kozuma, L. Deng, E. W. Hagley, J. Wen, R. Lutwak, K. Helmerson, S. L. Rolston, and W. D. Phillips, Phys. Rev. Lett. **82**, 871 (1999).
[7] E. W. Hagley *et al.*, Phys. Rev. Lett. **83**, 3112 (1999).
[8] Y. Torii, Y. Suzuki, M. Kozuma, T. Sugiura, T. Kuga, L. Deng, and E. W. Hagley, Phys. Rev. A **61**, R041602 (2000).
[9] J. E. Simsarian, J. Denschlag, M. Edwards, C. W. Clark, L. Deng, E. W. Hagley, K. Helmerson, S. L. Rolston, and W. D. Phillips, Phys. Rev. Lett. **85**, 2040 (2000).
[10] G. M. Moy, J. J. Hope, and C. M. Savage, Phys. Rev. A **55**, 3631 (1997).
[11] G. M. Moy and C. M. Savage, Phys. Rev. A **56**, R1087 (1997).
[12] C. M. Savage, J. Ruostekoski, and D. F. Walls, Phys. Rev. A **57**, 3805 (1998).
[13] C. K. Law and N. P. Bigelow, Phys. Rev. A **58**, 4791 (1998).
[14] R. J. Ballagh, K. Burnett, and T. F. Scott, Phys. Rev. Lett. **78**, 1607 (1997).
[15] H. Steck, M. Naraschewski, and H. Wallis, Phys. Rev. Lett. **80**, 1 (1998).
[16] H. Zeng, W. Zhang, and F. Lin, Phys. Rev. A **52**, 2155 (1995).
[17] J. Javanainen, Phys. Rev. A **54**, R4629 (1996).
[18] J. Ruostekoski and D. F. Walls, Phys. Rev. A **55**, 3625 (1997).
[19] J. Ruostekoski and D. F. Walls, Phys. Rev. A **56**, 2996 (1997).
[20] J. Steinbach, J. Twamley, and P. L. Knight, Phys. Rev. A **56**, 4815 (1997).
[21] J. Ruostekoski and D. F. Walls, Phys. Rev. A **59**, R2571 (1999).
[22] Z. Dutton, M. Budde, C. Slowe, and L. V. Hau, Science **293**, 668 (2001).
[23] K.-P. Marzlin, W. Zhang, and E. M. Wright, Phys. Rev. Lett. **79**, 4728 (1997).
[24] E. L. Bolda and D. F. Walls, Phys. Lett. A **246**, 32 (1998).
[25] J. E. Williams and M. J. Holland, Nature (London) **401**, 568 (1999).
[26] K.-P. Marzlin, W. Zhang, and B. C. Sanders, Phys. Rev. A **62**, 013602 (2000).
[27] G. Nandi, R. Walser, and W. P. Schleich, Phys. Rev. A **69**, 063606 (2004).
[28] K. T. Kapale and J. P. Dowling, Phys. Rev. Lett. **95**, 173601 (2005).
[29] J. Ruostekoski and J. R. Anglin, Phys. Rev. Lett. **86**, 3934 (2001).
[30] Z. Dutton and L. V. Hau, Phys. Rev. A **70**, 053831 (2004).
[31] Z. Dutton and J. Ruostekoski, Phys. Rev. Lett. **93**, 193602 (2004).
[32] J. Ruostekoski and Z. Dutton, Phys. Rev. A **72**, 063626 (2005); **73**, 039905(E) (2006).
[33] N. Tsukada, Phys. Rev. A **61**, 063602 (2000).
[34] Y. B. Band and M. Trippenbach, Phys. Rev. A **65**, 053602 (2002).
[35] J. Javanainen and J. Ruostekoski, Phys. Rev. A **52**, 3033 (1995).
[36] Y. Torii, Ph.D. thesis, University of Tokyo, 2000.
[37] For example, L. Allen and J. H. Eberly, *Optical Resonance and Two-Level Atoms* (Dover, New York, 1987).
[38] N. Watanabe and M. Tsukada, Phys. Rev. E **65**, 036705 (2002).
[39] T. Ando, Y. Ohtake, and N. Ohtani, Phys. Rev. E **73**, 066702 (2006).
[40] H. F. Trotter, Proc. Am. Math. Soc. **10**, 545 (1959).
[41] M. Suzuki, Phys. Lett. A **146**, 319 (1990).
[42] H. De Raedt and K. Michielsen, Comput. Phys. **8**, 600 (1994).
[43] T. Ando and M. Fujimoto, Phys. Rev. E **72**, 026706 (2005); **74**, 029902(E) (2006).
[44] D. A. Steck, *Rubidium 87 D Line Data*, rev. 1.6, 2003, [http://steck.us/alkalidata/rubidium87numbers.1.6.pdf].
[45] D. S. Hall, M. R. Matthews, J. R. Ensher, C. E. Wieman, and E. A. Cornell, Phys. Rev. Lett. **81**, 1539 (1998); D. S. Hall, M. R. Matthews, C. E. Wieman, and E. A. Cornell, *ibid.* **81**, 1543 (1998).
[46] We also performed calculations with $\Delta x = 100$ nm to find the incorrect OBD behavior, i.e., the decrease in the first-order diffraction peaks in the k_x spectra (Figs. 3–6) in larger $\tau_{\pi/2}$ regimes. To obtain correct results under the present calculation parameters, Δx must satisfy $\Delta x \leqslant 50$ nm.
[47] N. Watanabe and M. Tsukada, Phys. Rev. E **62**, 2914 (2000).
[48] H. Haug and S. W. Koch, *Quantum Theory of the Optical and Electronic Properties of Semiconductors*, 4th ed. (World Scientific, Singapore, 2004).